energies

Article

Nanofluid-Powered Dual-Fluid Photovoltaic/Thermal (PV/T) System: Comparative Numerical Study

M. Imtiaz Hussain [1], Jin-Hee Kim [1] and Jun-Tae Kim [2,*]

[1] Green Energy Technology Research Center, Kongju National University, 1223-24 Cheonan, Korea; imtiaz@kongju.ac.kr (M.I.H.); jiny@kongju.ac.kr (J.-H.K.)
[2] Department of Architectural Engineering, Kongju National University, 1223-24 Cheonan, Korea
* Correspondence: jtkim@kongju.ac.kr; Tel.: +82-41-521-9333

Received: 7 January 2019; Accepted: 22 February 2019; Published: 26 February 2019

Abstract: A limited number of studies have examined the effect of dual-fluid heat exchangers used for the cooling of photovoltaic (PV) cells. The current study suggests an explicit dynamic model for a dual-fluid photovoltaic/thermal (PV/T) system that uses nanofluid and air simultaneously. Mathematical modeling and a CFD simulation were performed using MATLAB® and ANSYS FLUENT® software, respectively. An experimental validation of the numerical models was performed using the results from the published study. Additionally, to identify the optimal nanofluid type for the PV/T collector, metal oxide nanoparticles (CuO, Al_2O_3, and SiO_2) with different concentrations were dispersed in the base fluid (water). The results revealed that the CuO nanofluid showed the highest thermal conductivity and the best thermal stability compared to the other two nanofluids evaluated herein. Furthermore, the influence of CuO nanofluid in combination with air on the heat transfer enhancement is investigated under different flow regions such as laminar, transition, and turbulent. Using a CuO nanofluid plus air and water plus air the total equivalent efficiency was found to be 90.3% and 79.8%, respectively. It is worth noting that the proposed models could efficiently simulate both single and dual-fluid PV/T systems even under periods of fluctuating irradiance.

Keywords: dual-fluid PV/T; nanofluid; numerical study; model validation

1. Introduction

Cooling the PV module with heat transfer fluids causes a decrease of the solar cells temperature and an increase of the electricity conversion efficiency. A compact heat exchanger having a smaller surface area would be an excellent choice to fulfill the specified amount of cooling required by the PV module. A conventional heat exchanger usually uses a single heat transfer fluid. Such heat exchangers have an insufficient contact area between the PV cells and the circulating fluids. Additionally, the PV module temperature increases due to the continuous penetration of solar radiation, which results in heat losses to ambient air [1]. For this reason, the optimization of the simultaneous production of heat energy and electricity from the PV/T system has been an important issue for the past two decades [2,3].

Over the years, the PV cells in PV/T collectors have been cooled using either water or air as the heat transfer fluid. Although air-based systems were demonstrated to be more economical for PV cell cooling, air has a relatively low heat transfer rate [4]. On the contrary, water-based systems, although more expensive, are considered more practical because of a higher thermal conductivity and a higher heat extraction rate compared to air [5,6]. The low thermal conductivity problem using water or air can be overcome by suspending nanoparticles in water. Adding nanoparticles into water results in a thermal conductivity improvement, and consequently, a significant positive effect on the heat transfer performance [7]. The effect of the different nanofluids on the thermal/electrical efficiency of the PV/T system was reported by Rejeb et al. [8]. It was found that under similar conditions, when nanofluids used as heat extraction fluids provide a better thermal and overall efficiency in comparison with water and ethylene glycol. Hasan et al. [9] introduced a nanofluid-based jet impingement system for PV panel cooling, where a nanofluid was directly injected to the rear surface of a PV panel by nozzles. The results showed that the application of a jet impingement using the nanofluid produced a higher thermal/electrical efficiency of the PV/T system than in the case of using water. For the purpose of performance enhancement, various researchers have tried to incorporate different types of colloidal solutions in PV/T systems [10–12]. Most of the aforementioned studies, however, were based on a single-fluid type heat exchanger.

These existing challenges related to efficient PV cooling can be handled by the simultaneous application of two fluids, e.g., water plus air. A dual-fluid heat exchanger for the PV/T system was reported for the first time by Tripanagnostopoulos [13]. He suggested that water plus air as a coolant can be circulated in the heat exchanger either simultaneously or independently depending on the energy needs. Abu Bakar et al. [14] later developed a 2-D steady state model of a dual-fluid PV/T system in which water and air were operated either independently or simultaneously. It was observed that a transverse arrangement of a serpentine-shaped copper tube to the air flow improves the heat extraction from the PV surface. Subsequently, Jarimi et al. [15] slightly modified the preceding model to make it suitable for a finned type air channel design. An experimental validation of the developed model was carried out using indoor test data. Furthermore, these studies were limited to steady state analyses.

This paper proposes transient mathematical and CFD models that are suitable for both dual-fluid and single-fluid type PV/T systems. To mix with water, four nanoparticles were chosen, among which the best was selected according to the maximum thermal/electrical performance of a PV/T collector. To increase the energy output per unit collector area, the influence of the optimal nanofluid in combination with air as a dual-fluid is further investigated. The PV/T system is designed in such a way that both heat extraction fluids can be operated independently and simultaneously. In the independent mode of fluid operation, either of the two heat transfer fluids is operated, whereas in the simultaneous mode both heat transfer fluids are operated at the same time. Additionally, the thermal and overall performance of the proposed dual-fluid PV/T collector is evaluated in comparison with the performance of the PV/T collector based on conventional fluids.

2. Collector Design

The dual-fluid PV/T system integrates a standard mono-crystalline silicon PV panel (Table 1) with a conventional parallel tube heat exchanger and a single pass air heater, as depicted in Figure 1. A schematic diagram of the back panel assembly with flow paths of both heat transfer fluids in the PV/T collector is presented in Figure 2. The system is designed such that the nanofluid and air are forced to circulate in the copper tubes and an air duct, respectively, both independently and simultaneously. The outer surface of the tube absorber is intentionally corrugated to increase the heat transfer surface area. Furthermore, to increase emissivity, the interior of the back panel including the PV rear surface is explicitly considered to be black. In this study, a similar sheet and tube type heat exchanger was taken into consideration, as explained in the references [16,17], except for the absorber plate that is normally used between the PV laminate and the fluid pipe. Instead, the tubes are directly attached to the rear surface of the PV laminate using a thermal epoxy, as suggested by Abu Bakar et al. [14]. Due to direct contact with the tube absorber, the heat transfer rate from the PV module surface to the circulating fluids will be increased.

Table 1. Specification of the PV module.

Cell Type	Mono-Crystalline Silicon
Open circuit voltage	38.1 V

Table 1. *Cont.*

Cell Type	Mono-Crystalline Silicon
Short circuit current	9.27 A
Maximum power point	31.6 V & 8.23 A

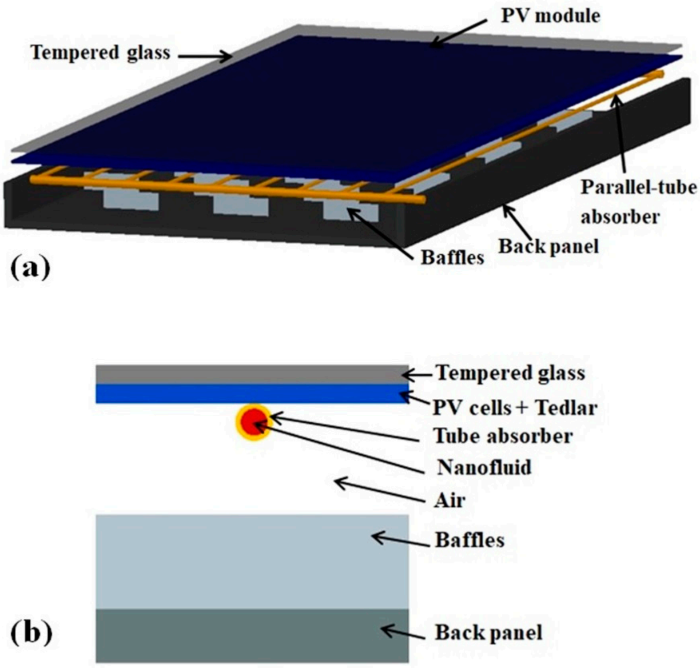

Figure 1. Dual fluid PV/T collector: (**a**) exploded view, and (**b**) cross-section view considering a single pipe.

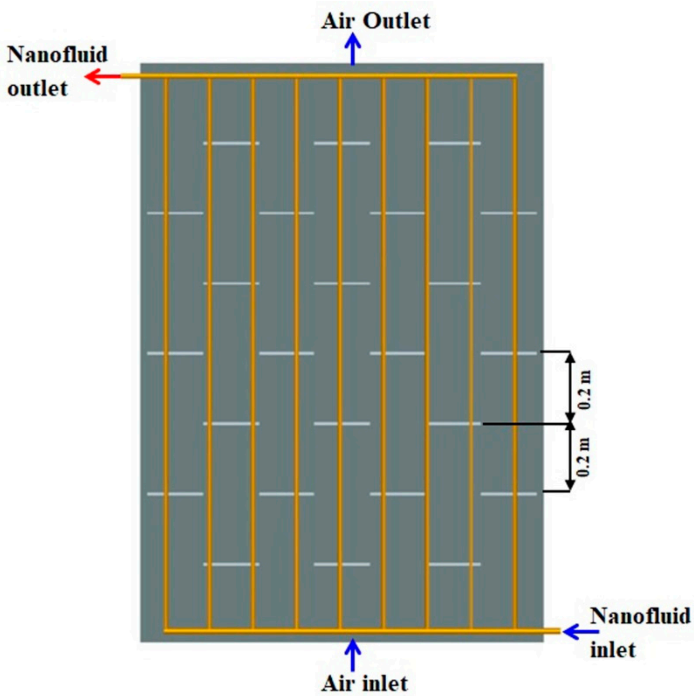

Figure 2. The back panel front view and the flow paths of both fluids.

A series of baffles were arranged on the back plate surface at a certain distance transverse to the air flow direction, for the purpose of breaking the laminar sub-layer between the channel walls and the circulating air, and thereby reduce the thermal resistance. This arrangement will significantly increase the heat transfer interactions among the different components within the back panel of the PV/T collector.

3. Mathematical Model

The proposed model of the dual-fluid PV/T is developed by modifying the single-fluid PV/T model reported by Chow [18]. The transient energy balance equations across different collector components were modified according to a dual-fluid PV/T design. The explicit dynamic model can viably be applied to both single- and dual-fluid PV/T systems. The parameters that were used for the simulation are given in Table 2. In the simulation, a control volume having a fictitious boundary is regarded as a node within which the mass and energy balances are satisfied [5]. Along the flow direction, the heat is accumulated, which leads to a positive temperature gradient in all of the collector components. Due to the parallel arrangement, the fluid flow rate is assumed to be the same in all the copper tubes. The material properties and physical dimensions of the PV plate, copper tubes, and back panel are considered to be constant [18]. All the heat transfer coefficients used for the simulation are calculated in real time.

Table 2. Data for the simulation.

PV module [14]	Length & width	1.62 m & 0.98 m
	Absorptivity (α_p)	0.9
	Emissivity (ε_p)	0.88
	Specific heat (C_p)	900 J/(kg·K)
	Temperature coefficient (β_r)	0.0045/°C
	Reference PV panel temperature	298.15 K
Absorber tube	Inner diameter (D_i)	0.008 m
	Thickness (δ_t)	0.0012 m
	Specific heat (C_t)	903 J/(kg·K)
	Density (ρ_t)	2702 kg/m^3
	No. of tubes	9
	Tube spacing	0.11 m
	Material	Copper
Back panel	Density (ρ_b)	20 kg/m^3
	Specific heat (C_b)	670 J/(kg·K)
	Thermal conductivity (K_b)	0.034 W/(m·K)
Nanoparticles used	CuO, Al_2O_3, and SiO_2	-
Other fluids used	Water & air	-

In the PV/T system, the temperature change across the interface between the layers of different materials is attributed to the thermal resistance. Therefore, each component of the collector can be represented by a temperature node. The first node, '*p*', represents the PV plate, the '*t*' node represents the tube absorber, '*n*' is for the nanofluid in the tube, '*a*' is for the inside air, and the last node, '*b*', denotes the back panel.

3.1. PV Plate

$$M_pC_p(dT_p/dt) = G\alpha_p - E - h_{wind}A_{p\infty}(T_p - T_\infty) - h_{p\infty}A_{p\infty}(T_p - T_\infty) - h_{pt}A_{pt}(T_p - T_t) \\ - A_{pa}\,h_{pa}(T_p - T_a) - h_{pb}A_{pb}(T_p - T_b) \quad (1)$$

where α_p is the absorptivity of the PV plate; M_p, T_p, and C_p are the mass, temperature, and specific heat of the PV plate, respectively; G and E are the solar radiation and electrical output from the PV cells, respectively; and T_∞, T_t, T_a, and T_b are the ambient, absorber tube, inside air, and back panel temperatures, respectively. h_{wind} is the heat convected caused by wind [19], $h_{p\infty}$ is the heat radiated from the PV plate to ambient air, h_{pt} is the energy conducted from the PV plate to the absorber tube, h_{pa} is the heat convected from the PV plate to inside air, and h_{pb} is the heat radiated from the PV plate to the back panel.

$$E = GP\eta_e \tag{2}$$

$$\eta_e = \eta_r[1 - \beta_r(T_p - T_r)] \tag{3}$$

where P and η_e are the packing factor and electrical efficiency, respectively. β_r and η_r are respectively the temperature coefficient and cell efficiency at the reference operating temperature (T_r).

$$h_{wind} = 3u_a + 2.8 \tag{4}$$

$$h_{p\infty} = \varepsilon_p\sigma(T_p + T_\infty)\left(T_p^2 + T_\infty^2\right) \tag{5}$$

$$h_{pb} = \left(\sigma(T_p + T_b)\left(T_p^2 + T_b^2\right)\right)/(1/\varepsilon_p + 1/\varepsilon_b - 1) \tag{6}$$

$$h_{pt} = 2k_p/x_p \tag{7}$$

$$x_p = (W - D_o)/4 \tag{8}$$

where u_a is the wind velocity and k_p is the thermal conductivity of the PV plate. ε_p and ε_b are the emissivity of the PV plate and back panel, respectively. W is the tube spacing [18], and D_o is the outer diameter of the tube.

3.2. Absorber Tube

$$M_tC_t(dT_t/dt) = h_{pt}A_{pt}(T_p - T_t) - A_{tn}\,h_{tn}(T_t - T_n) - A_{ta}\,h_{ta}(T_t - T_a) - h_{tb}A_{tb}(T_t - T_b) \tag{9}$$

where C_t and M_t are the specific heat and mass of the absorber tube, respectively; h_{tn} and h_{ta} represent the heat convected from the tube to the nanofluid and inside air, respectively; and h_{tb} is the heat radiated from the tube to the back panel. h_{tn} can be estimated using the following correlation [8]:

$$h_{tn} = Nu_n k_n/D_i \tag{10}$$

where k_n and Nu_n are the thermal conductivity and Nusselt number of the nanofluid.

Assuming a spherical shape of Al_2O_3 nanoparticles [20], the Nusselt number can be calculated as follows:

$$Nu_n = Pr^{0.1039}\left(1.0257\phi + 1.1397Re^{0.205} + 0.788\phi Re^{0.205} + 1.2069\right) \tag{11}$$

where ϕ represents the volume concentration of metal oxide nanoparticles in the water. Pr and Re are the Prandtl number and Reynolds number, respectively.

Nanofluid in tube

$$M_nC_n(dT_n/dt) = \dot{m}_nC_n\,(T_{n,o} - T_{n,in}) + A_{tn}\,h_{tn}(T_t - T_n) \tag{12}$$

$$T_n = (T_{n,o} + T_{n,in})/2 \tag{13}$$

where $\dot{m}_n$ is the (mass) flow rate of the nanofluid. C_t and M_t are respectively the specific heat and mass of the nanofluid. $T_{n,in}$ and $T_{n,o}$ are respectively the nanofluid inlet and outlet temperatures.

Inside air

$$M_aC_a(dT_a/dt) = \dot{m}_aC_a\,(T_{a,o} - T_{a,in}) + A_{pa}\,h_{pa}(T_p - T_a) + A_{ta}\,h_{ta}(T_t - T_a) + h_{ab}A_{ab}(T_a - T_b) \tag{14}$$

$$T_a = (T_{a,o} + T_{a,in})/2 \tag{15}$$

where $\dot{m}_a$ is the (mass) flow rate of the inside air; C_a and M_a are respectively the specific heat and mass of the inside air; $T_{a,in}$ and $T_{a,o}$ are respectively the air inlet and outlet temperatures; and h_{ab} is the convected heat from the back panel to the inside air.

3.3. Back Plate

$$M_b C_b (dT_b/dt) = h_{tb} A_{tb} (T_t - T_b) + h_{pb} A_{pb} \left(T_p - T_b\right) - h_{ab} A_{ab} (T_a - T_b) - h_{b\infty} A_{b\infty} (T_b - T_\infty) \tag{16}$$

where C_b and M_b are respectively the specific heat and mass of the back panel; and $h_{b\infty}$ is the heat loss to ambient air. The instantaneous total thermal efficiency of the dual-fluid PV/T collector is determined using the following correlation [4]:

$$\eta_{th} = \frac{\dot{m}_n C_n \ (T_{n,o} - T_{n,in}) + \ \dot{m}_a C_a \ (T_{a,o} - T_{a,in})}{A_c G} \tag{17}$$

where A_c is the collector area, which is considered to be the same as the PV plate area (A_p). The total yield of the dual-fluid PV/T system can be expressed in terms of primary energy saving efficiency or total equivalent efficiency. For this purpose, the electrical efficiency of the PV/T system is divided by the efficiency of a conventional electric power plant [15]. The total equivalent efficiency is calculated as follows:

$$\eta_{PVT} = \eta_{th} + \eta_e/\eta_{pp} \tag{18}$$

where η_{PVT} is the total equivalent efficiency and η_e is the electrical efficiency. An η_{pp} average value of 38% is taken as the electric generation efficiency for a coal power plant [19]. As suggested by Maxwell [21], the thermal conductivity of the colloidal solution (nanofluid) can be expressed as:

$$k_n = \frac{\left[\left(k_{np} + k_{bf}\right) + 2\phi + \left(k_{np} - k_{bf}\right)\right]}{\left[\left(k_{np} + k_{bf}\right) - \phi\left(k_{np} - k_{bf}\right)\right]} \tag{19}$$

Considering the mixture rule [22], the equation for calculating the nanofluid density can be written as:

$$\rho_n = \rho_{np}(\phi) + \rho_{bf}(1 - \phi) \tag{20}$$

The specific heat of the nanofluid can be determined as follows [22]:

$$C_n = C_{np}(\phi) + C_{bf}(1 - \phi) \tag{21}$$

where, ρ_n is the density of the nanofluid. The subscripts np and bf are denoted as the nanoparticles and base fluid, respectively.

4. CFD Model

In order to analyze the performance of a dual-fluid PV/T system, the temperature distribution in the cooling conduits and the PV module was predicted using the model built in ANSYS FLUENT software (Release 14.5, ANYSY, Inc., Canonsburg, PA, USA) [23]. The CAD modeling of the proposed system was performed using Creo Elements/Pro software. A precise and accurate prediction of the temperature profile across the PV module plays a key role in developing a prototype of a complex solar system such as a dual-fluid PV/T system [24]. Therefore, in this study, special care was taken regarding the selection of boundary conditions and discretization schemes. Modeling and a numerical analysis have been performed based on the following three steps. The first step is to develop a dual-fluid PV/T model. The second step is assessing the thermal performance of the collector under various operating conditions. The last step is the validation of the developed model using experimental data.

4.1. Numerical Scheme

A computational fluid dynamics (CFD) solver based on the finite volume method (FVM) was used to discretize the continuous governing equations into algebraic counterparts [25]. To provide the solution field, these algebraic counterparts are then solved numerically. To produce the velocity and temperature field solutions, different convergence criteria were set; the convergence of the continuity and momentum equations and energy equation is achieved when the residuals drop to 10^{-3} and 10^{-6}, respectively. To enhance the solution stability and to accelerate the convergence rate, the under relaxation factors were precisely taken. The temperature condition and fluid flow rate in the parallel tubes can be considered as being the same; the model is therefore limited to the vicinity of a single tube [26,27].

To evaluate the heat flow through the fluid-solid interactions, a conjugate heat transfer mechanism was taken into account [28]. For this purpose the whole model is divided into two domains based on their physical appearance: the solar cells, absorber tube, baffles, and back panel compose a solid domain, while the air and the nanofluid or water compose a fluid domain. The domains are differentiated by different colors, as shown in Figure 1b. A no-slip condition was imposed at all the fluid-solid boundaries. The *k-ε* two-transport-equation model with an enhanced wall treatment was chosen to solve and analyze the turbulence in the air duct and nanofluid pipe. The governing equations used to define the velocity, pressure, and temperature in the fluid domain is as follows [29]:

Continuity equation:

$$\frac{\partial u}{\partial x} + \frac{\partial v}{\partial y} + \frac{\partial w}{\partial z} = 0 \tag{22}$$

Momentum equation:

$$\left(u\frac{\partial u}{\partial x} + v\frac{\partial u}{\partial y} + w\frac{\partial u}{\partial z} \right) = -\frac{1}{\rho}\frac{\partial p}{\partial x} + \mu\left\{ \frac{\partial^2 u}{\partial x^2} + \frac{\partial^2 u}{\partial y^2} + \frac{\partial^2 u}{\partial z^2} \right\} \tag{23}$$

$$\left(u\frac{\partial v}{\partial x} + v\frac{\partial v}{\partial y} + w\frac{\partial v}{\partial z} \right) = -\frac{1}{\rho}\frac{\partial p}{\partial y} + \mu\left\{ \frac{\partial^2 v}{\partial x^2} + \frac{\partial^2 v}{\partial y^2} + \frac{\partial^2 v}{\partial z^2} \right\} \tag{24}$$

$$\left(u\frac{\partial z}{\partial x} + v\frac{\partial z}{\partial y} + w\frac{\partial z}{\partial z} \right) = -\frac{1}{\rho}\frac{\partial p}{\partial z} + \mu\left\{ \frac{\partial^2 w}{\partial x^2} + \frac{\partial^2 w}{\partial y^2} + \frac{\partial^2 w}{\partial z^2} \right\} \tag{25}$$

Energy equation

$$u\frac{\partial T}{\partial x} + v\frac{\partial T}{\partial y} + w\frac{\partial T}{\partial z} = \alpha\left\{ \frac{\partial^2 T}{\partial x^2} + \frac{\partial^2 T}{\partial y^2} + \frac{\partial^2 T}{\partial z^2} \right\} \tag{26}$$

u_i is velocity field u, v, w along x, y, z.

4.2. Boundary Conditions and Grid Study

A mass flow rate boundary condition was used at the tube absorber and air channel entrances, respectively. A pressure-outlet boundary condition was applied at the outlet section of both fluids. For the analysis, the ambient air temperature was considered to be 25 °C and the incident solar radiation of 900 W/m^2 was taken into account. Due to the opaque top surface of the PV/T collector, a fixed heat flux was applied as a thermal boundary condition instead of using a solar ray tracing algorithm, because the solar load model's ray tracing algorithm in FLUENT does not include the internals such as the heat gain for a model having an opaque rooftop [30].

For the appropriate meshing, an automatic mesh method, which is the toggle between tetrahedron (patch conforming algorithm) and sweep meshing, has been used. A higher density mesh was applied in the areas where the heat transfer is of greater concern. In order to obtain the desired solution, a grid independence test was carried out, in particular for those problems where the heat transfer fluid phenomenon is involved. In this study, different grid sizes were tested by taking into account the PV module temperature. The goal of this step is to ensure that the predicted PV temperature will no longer be changed by varying the size of the grid. The process to find the optimal mesh size is also known as a grid independence study. Four grid sizes with 781,430, 903,638, 1,060,023, and 1,437,673 element numbers were tested for the given dual-fluid PV/T model, as shown in Table 3. The optimal mesh size for the independent and simultaneous fluid modes are found to be 903,638 and 1,060,023 element numbers, respectively.

Table 3. A grid independency test.

Number of Elements	PV Module Temperature (°C)			
	Water	Nanofluid	Water + Air	Nanofluid + Air
781,430	57.46	56.18	50.69	46.65
903,638	59.35	57.47	51.55	48.42
1,060,023	60.16	58.73	52.39	47.44
1,437,673	59.87	57.92	52.23	47.37

5. Results and Discussion

5.1. Model Validation

The dual-fluid PV/T model has been validated individually for the air and the nanofluid heat transfer fluids. This means that the air flow rate is set to zero when the nanofluid is to be operated, and vice versa when the air is operated independently. The model validation was performed by comparing the predicted PV and outlet air temperatures against the experimental data for the unglazed PV/T air heating system presented by Joshi et al. [31]. For the purpose of the comparison, similar geometric and operational parameters were considered, as indicated in the reference [31]. Other information that is not given in this research was taken from the study by Abu Bakar et al. [14]. As can be seen in Figure 3, the maximum deviation between the predicted and measured values did not exceed 2.25 °C and 1.98 °C for the PV and outlet air temperatures, respectively. These deviations can be attributed to the assumptions made during the model development. The published data have a satisfactory agreement with the simulation results delivered by the suggested model.

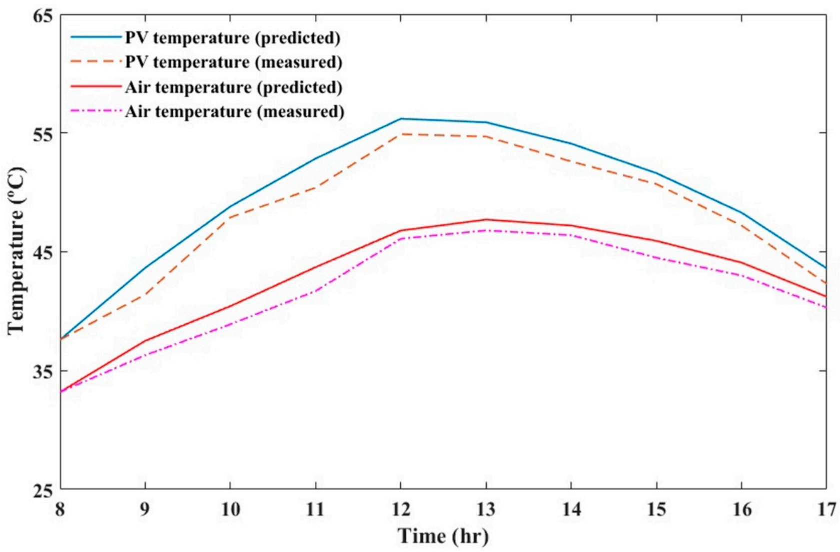

Figure 3. The simulated results by model against experimentally measured data from a previous study.

Meanwhile, the numerical model of a nanofluid heat exchanger was validated by comparing the predicted results with the experimental data taken from the uncovered nanofluid PV/T system reported by Rejeb et al. [8]. To check the reliability of the model, a statistical parameter, the root mean square percentage deviation (RMSD), is used [15]. The RMSD, which is the most frequently used parameter for error analysis, measures the deviations between the results predicted by a model and the measured results. The RMSD for the average PV surface and nanofluid outlet temperatures between the predicted and measured data was found to be 1.3% and 1.9%, respectively. The results derived from the model are consistent with the experimental data. It is concluded that the obtained results demonstrate the reliability of the model that is used for the performance prediction of the PV/T system.

$$RMSD = \left(\frac{1}{n} \sum_{i=1}^{n} (Y_i - X_i)^2 \right)^{1/2} \tag{27}$$

where n is the number of data points. Y_i and X_i are the predicted and measured values, respectively.

5.2. Results Derived from Mathematical Model

The selection of an optimal fluid type and the optimal concentration of nanoparticles are important for a higher energy production from the PV/T collector. Based on the availability, cost, and inertness to the PV/T material, three metal oxide nanoparticles were selected: aluminum oxide (Al_2O_3), copper oxide (CuO), and silicon dioxide (SiO_2). Table 4 shows the thermo-physical properties of the metal oxide nanoparticles used in this study [32–34]. The influence of the nanoparticle concentrations on the collector's performance is investigated by considering important thermo-physical properties such the viscosity and thermal conductivity. As depicted in Figure 4, the viscosity ratio and thermal conductivity ratio increase with the increasing nanoparticle concentration. However, the highest percentage increase in the thermal conductivity was found with the CuO nanofluid, followed by the Al_2O_3, and SiO_2 nanofluids. The optimal concentration for the available nanoparticles in the base fluid (water) is around 0.75%; beyond this point, the aggregation of the nanoparticles and thermal diffusivity increased significantly. One of the reasons that the CuO nanofluid affords the highest heat transfer performance is that it has a lower specific heat and a slightly higher thermal conductivity compared to the aforementioned nanofluids. Based on the preceding outcomes, the CuO nanoparticles with a concentration of 0.75% in water are selected and employed as an optimal nanofluid throughout the rest of this study.

Table 4. The thermo-physical properties of metal oxides.

Metal Oxides or Additive	Chemical Formula	Properties		
		Specific Heat (J/kg·K)	Thermal Conductivity (W/m.K)	Density (kg/m^3)
Copper oxide	CuO	551	32.9	6310
Aluminum oxide	Al_2O_3	773	30	3890
Silicon dioxide	SiO_2	730	1.5	2650

In order to locate the optimal flow rate of each fluid, both the nanofluid and air are operated independently when their counterparts are kept stagnant. Considering the proposed system configurations, the laminar, transition, and turbulent flow regions for the nanofluid are 0.006 kg/s, 0.015 kg/s, and 0.025 kg/s, respectively; and for air, they are 0.009 kg/s, 0.024 kg/s and 0.055 kg/s, respectively. Therefore, the mass flow rate of the nanofluid varied from 0 to 0.03 kg/s, and the air flow rate from 0 to 0.1 kg/s. The thermal and electrical efficiencies of the PV/T collector are predicted by operating the CuO nanofluid and air independently, as shown in Figure 5. The efficiency values increased with an increasing flow rate of both fluids. However, the impact of the increase of the air flow rate on the PV/T efficiency patterns is small compared to the nanofluid flow rate. Furthermore, the percentage increase of the thermal and electrical efficiencies with the air flow rate is very small. On the contrary, the increase in the collector efficiency is notable even at a low mass flow rate of the nanofluid. Therefore, due to better thermal properties and a high heat removal capability, the nanofluid flow rate varied, as opposed to the air flow rate. This means that when both heat transfer fluids were operated simultaneously, the air flow was kept constant while the variable flow rate of the CuO nanofluid was considered.

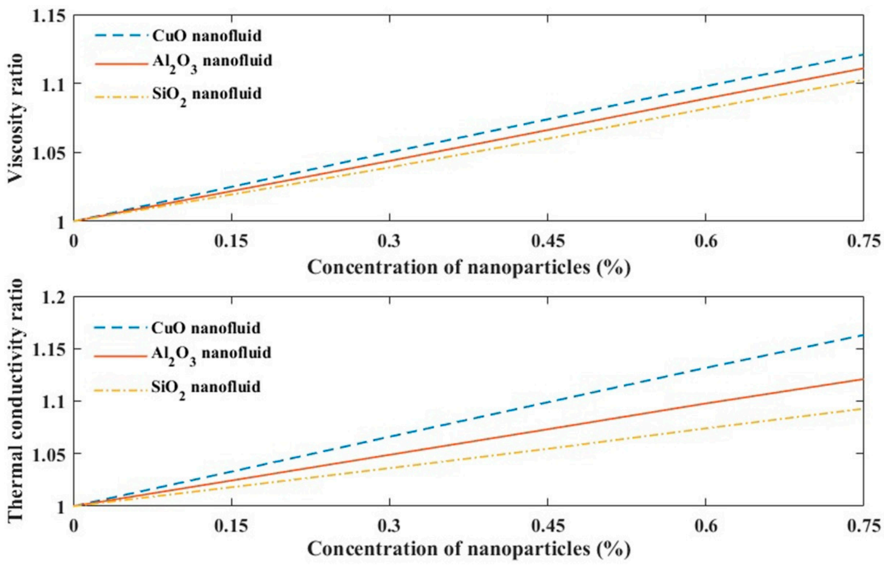

Figure 4. Variations of viscosity and thermal conductivity ratios with increasing concentrations of CuO, Al_2O_3, and SiO_2 nanoparticles in pure water.

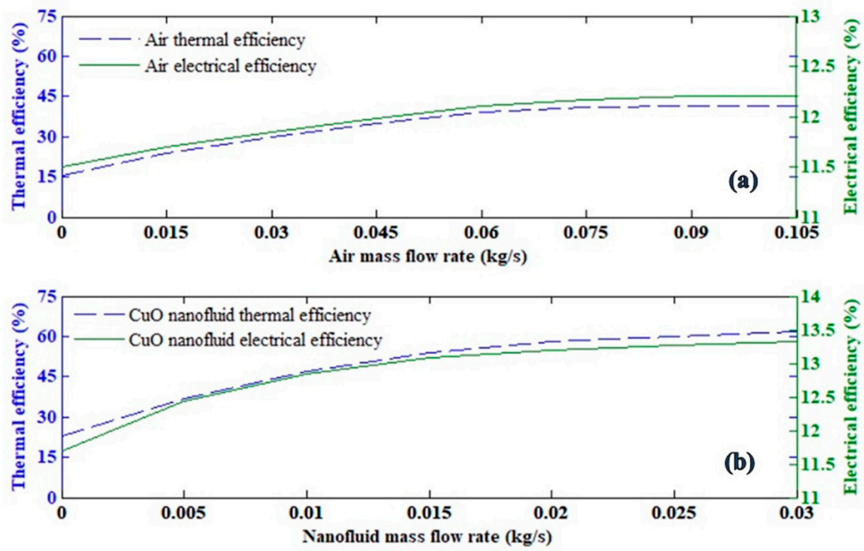

Figure 5. The predicted efficiencies of the PV/T efficiency at the independent mode of fluid operation: (**a**) stagnant CuO nanofluid; and (**b**) stagnant air.

Considering different heat transfer fluids, the daily PV module temperature is predicted under similar operating conditions. For a comparative analysis, four fluid modes were used: water, CuO nanofluid, water plus air, and CuO nanofluid plus air (Figure 6). During the simultaneous mode of fluid operation, the air and CuO nanofluid flow rates were fixed at 0.055 kg/s and 0.025 kg/s, respectively. During the independent mode, the flow rate of either one of the two heat transfer fluids was set to zero, as described by Abu Bakar et al. [14]. The predicted results show that the maximum PV module temperature with water, nanofluid, air plus water, and air plus nanofluid was 57.5 °C, 55.1 °C, 51.9 °C, and 48.6 °C, respectively. It is noted that the nanofluid (in either the simultaneous or independent mode) has an enormous potential as a heat transfer fluid compared to water. This indicates that a fluid with a high thermal conductivity can extract extra accumulated solar heat from PV cells and thus provide better and more targeted cooling. In addition, the simultaneous application of two fluids (air and nanofluid in particular) results in a significant reduction in the PV cell temperature. The results showed that the application of two fluids remarkably enhanced the total surface area of the heat exchanger. It should be noted that when a dual-fluid heat exchanger is used for the independent mode of fluid operation, it might affect the secondary fluid outlet temperature due to the primary fluid which may have been trapped in the pipe bends.

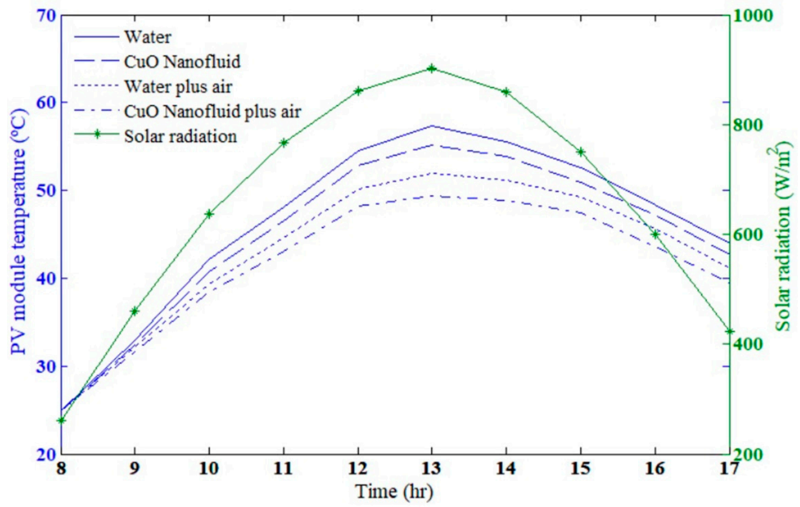

Figure 6. The daily predicted PV module temperature using different fluids and modes of fluid operations.

The influence of the variable flow rate of the nanofluid or water at a fixed airflow on the fluid temperature rise is presented in Figure 7. When the fluids are to be circulated simultaneously, the temperature rise of both fluids decreased as the flow rate of the nanofluid increased. During the simultaneous operation of fluids, the temperature rise of both the CuO nanofluid and air was higher than the water and air. In both systems, the temperature rise of the liquid fluids (nanofluid and water) was smaller than that of the air. The discrepancy may be a result of the lower specific heat capacity of air. In addition, the findings demonstrate that the CuO nanofluid in combination with air can extract more accumulated solar heat from the PV/T system than water and air as a dual-fluid. This is anticipated to be due to the higher thermal conductivity and the lower specific heat of the nanofluid by dispersing CuO to the water, which removes solar heat faster than water.

Table 5 shows the variations of the total equivalent efficiency of a dual-fluid PV/T system against the variable CuO nanofluid flow rate at a fixed airflow of 0.055 kg/s. Meanwhile, the total equivalent efficiency is determined at a fixed quantity of the daily solar radiation (23.25 MJ/m^2 day) and ambient temperature (21.47 °C). When the nanofluid flow rate is set to vary between 0.005 kg/s and 0.030 kg/s at a fixed air flow rate of 0.055 kg/s, the total equivalent efficiency of the PVT collector was increased to 79.8% and 90.3% with water plus air, and with nanofluid plus air, respectively. It is noted that at the lowest nanofluid flow rate of 0.005 kg/s, the total equivalent efficiency was found to be as low as 82.6%, while under similar operating conditions using water plus air, the minimum value was 73.7%. The results show that when the fluids are operated simultaneously, a reasonably good total equivalent efficiency is achievable even at a low mass flow rate. In comparison with water plus air, the total equivalent efficiency of the PV/T system using nanofluid plus air as the dual-fluid was found to be approximately 10% higher. This can be attributed to the thermophysical properties of the nanofluid being sufficiently great to enhance the heat transfer behavior and thus increase the rate of heat removal from the PV module.

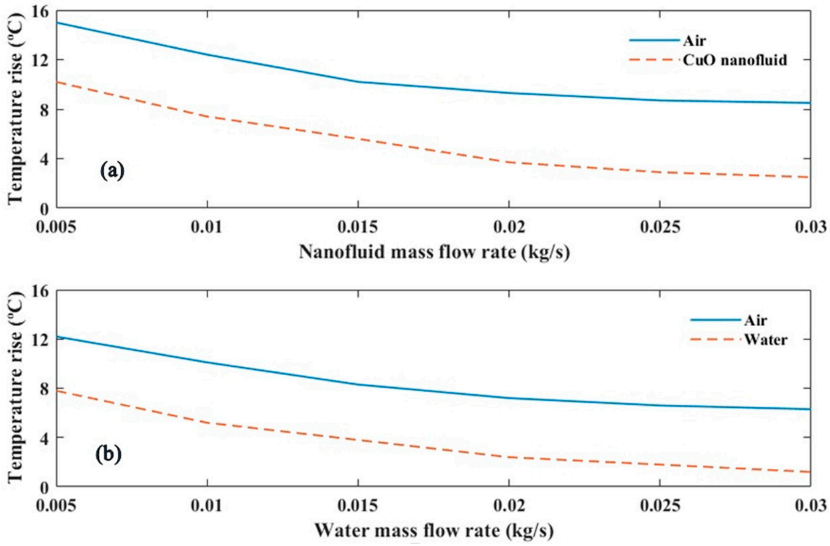

Figure 7. The predicted fluids temperature rise against variable: (**a**) nanofluid mass flow rate, and (**b**) water mass flow rate at fixed air flow rate (0.055 kg/s).

Table 5. Total equivalent efficiency of the dual-fluid PV/T system.

Nanofluid or Water Flow Rate (kg/s)	Fixed Air Flow Rate (kg/s)	Daily Solar Radiation (MJ/m^2 day)	Ambient Temperature (°C)	Total Equivalent Efficiency (%)		
				PV without Cooling	Water Plus Air	Nanofluid Plus Air
0.005	0.055	23.25	21.47	31.5	73.7	82.6
0.01	0.055	23.25	21.47	-	75.1	85.2
0.015	0.055	23.25	21.47	-	76.6	87.4
0.02	0.055	23.25	21.47	-	78.4	88.7
0.025	0.055	23.25	21.47	-	79.1	89.5
0.03	0.055	23.25	21.47	-	79.8	90.3

5.3. Results Derived from CFD Model

Figure 8 shows the variations of the convection heat transfer coefficient for various fluid flow rates and absorber temperatures. The convection heat transfer coefficient is calculated using the fluid average temperature and wall temperature, which are extracted from the ANSYS FLUENT software. To understand the influence of the nanofluid, the convection heat transfer coefficients of the CuO nanofluid (0.45%, 0.60%, and 0.75%) are discussed here, in comparison with those of water. The results indicate that the convection heat transfer coefficient (h_ft) between the circulating fluid and absorber wall increases for all heat transfer fluids with an increasing mass flow rate, as expected. However, initially, at an absorber temperature of 55 °C, the water shows a higher h_ft than that of the CuO nanofluid. The high specific heat of water may at least partly account for these results. Moreover, the low density and high thermal conductivity of the CuO nanofluid at a higher temperature enhances the random motion of the nanoparticles, and this ultimately results in an increase of the nanoparticle contact with the absorber surface and the heat transfer rate, respectively. It is observed that at a higher absorber temperature of 95 °C, the 0.75% CuO nanofluid has the highest heat transfer rate, followed by 0.60% CuO, 0.45% CuO, and water.

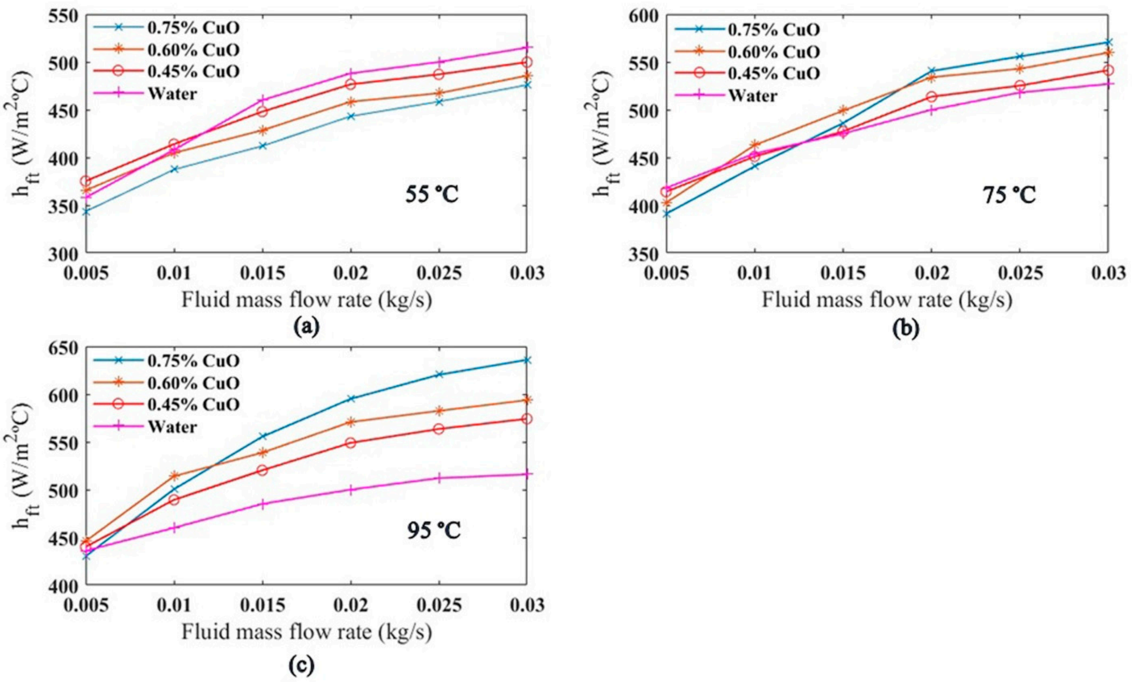

Figure 8. The variations of the heat transfer coefficient for different mass flow rates at absorber temperatures of (**a**) 55 °C, (**b**) 75 °C, and (**c**) 95 °C.

Since the absorber tubes are arranged in parallel, the temperature distribution and fluid flow through all the tubes can be taken as being the same. Therefore, the vicinity of a single pipe can be used to analyze the thermal behavior of the entire PV panel [18]. The temperature distribution across the PV surface is predicted under the simultaneous and independent modes of fluid operation, namely: water, CuO nanofluid, water plus air, and CuO nanofluid plus air. In the simulation, the flow rates of the liquid fluid and air are considered to be fixed at 0.025 kg/s and 0.055 kg/s, respectively. The interface temperature between the PV module and both heat exchangers is presented in Figures 9 and 10. Due to the fluid-to-solid and solid-to-solid coupling, the shadow effects can be clearly seen at the interfaces or common faces. The PV surface temperature has been reported taking four modes of fluid operation into account: with solely a water heat exchanger, the PV surface reached a temperature of 59 °C; with the use of the nanofluid, the estimated PV surface temperature is 56 °C; with water plus air as a dual exchanger, the PV temperature fell to 52 °C; and with nanofluid plus air this value further declined to 47 °C. This is attributed to the dual-fluid exchanger possibly covering most of the surface area of the PV module and ultimately contributing to a more efficient heat transfer. Furthermore, in the case of the simultaneous application of nanofluid plus air, in particular, an increase in the surface area of the heat exchanger is one among other possible explanations.

It is worthwhile to investigate the thermal performance of each fluid in a dual-fluid PV/T system when both fluids are operated at the same time, as shown in Figures 11 and 12. In particular, a combination of the CuO nanofluid and air as a dual fluid is attractive because of the superior thermo-physical properties of the nanofluid relative to those of water. Because of the simultaneous operation, the thermal performance of each fluid is directly associated with its counterpart. Therefore, it is worth noting the contribution of each fluid to the overall performance of a dual-fluid PV/T system. In a situation where the mass flow rate of water or nanofluid increases while considering a fixed air flow rate, the extra solar heat is extracted by the fluid with an increasing flow rate [15]. Therefore, a relatively small amount of solar heat remains to be removed by air as a second fluid. The observed increase in the mass flow rate of the nanofluid or water at a constant air flow rate had a significant impact on the amount of heat extracted by air. Hence, the total amount of accumulated solar heat extracted by a nanofluid plus air is higher than in the case of water plus air when used as a dual fluid.

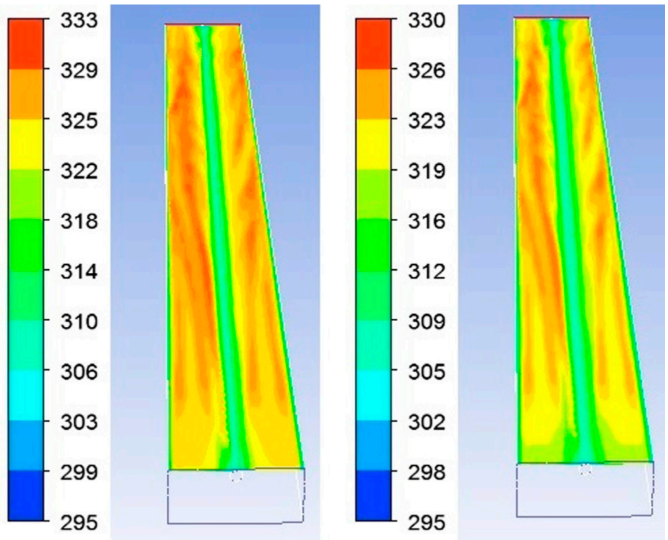

(a) (b)

Figure 9. The PV module temperature (K) distribution under the independent mode of fluid operation (**a**) with water only, and (**b**) with nanofluid only.

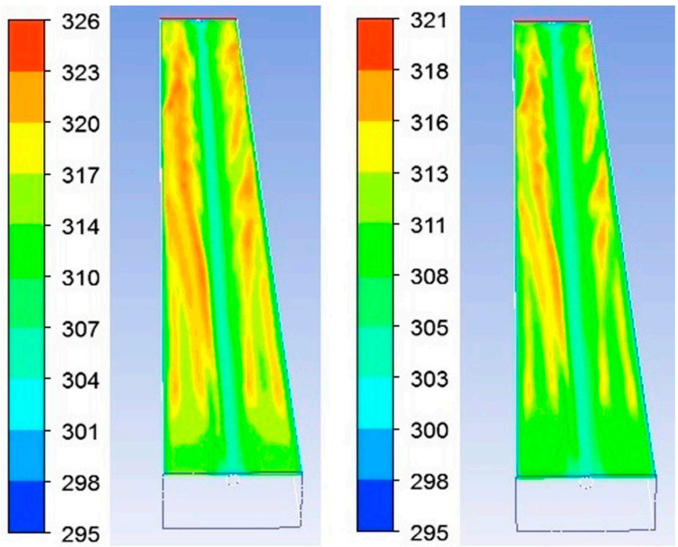

(a) **(b)**

Figure 10. The PV module temperature (K) distribution under the simultaneous mode of fluid operation (**a**) with water plus air, and (**b**) with nanofluid plus air.

The nano-engineered dual-fluid PV/T system is assessed in terms of effectiveness and reliability by comparing its performance with the previously reported collectors using conventional heat transfer fluids such as air, water, nanofluid, and water plus air (Figure 13). As reported by Abu Bakar et al. [14], the maximum thermal and electrical efficiencies of the PV/T collector with water plus air were 65.1% and 11.3%, respectively. In contrast, using the proposed PV/T collector, the predicted thermal and electrical efficiencies were found to be 8.4%, and 2.3%, respectively, higher than those of the aforementioned case. Compared to water-based and nanofluid-based PV/T systems [11], the proposed system had a 26%, and 17.3% higher thermal efficiency, respectively. Furthermore, in the case of the reference PV module (without cooling) [35], the electrical efficiency was found to be 6.61%. This may be attributed to the use of two fluids for the PV cells cooling, which consequently increased the overall surface area for the heat transfer, and hence ultimately improved the heat extraction from the PV cells. Specifically, introducing the CuO nanofluid along with air as a dual fluid increases the total efficiency per unit area because of their superior thermo-physical properties. Using the CuO nanofluid in combination with air for a PV/T system is promising considering the higher overall performance that can be achieved compared to a collector employing conventional fluids. In addition, a nano-engineered dual-fluid PV/T system offers a wide range of thermal applications depending upon the energy needs.

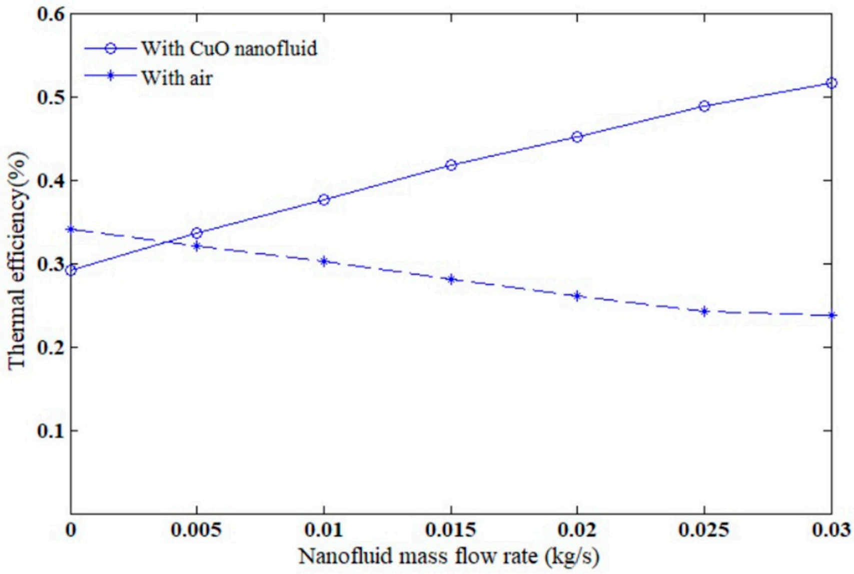

Figure 11. Variations of dual-fluid PV/T thermal efficiencies under the simultaneous fluid mode against a variable nanofluid flow rate at a fixed air flow rate (0.055 kg/s).

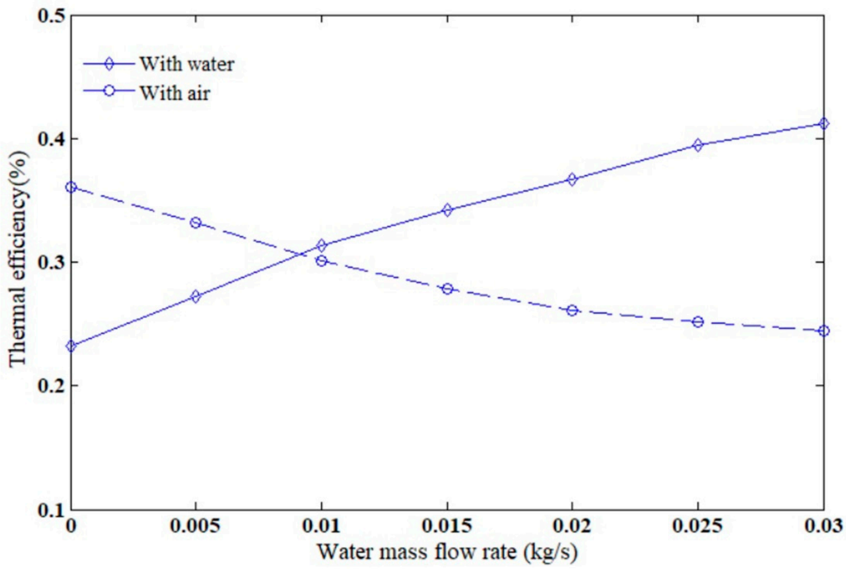

Figure 12. Variations of dual-fluid PV/T under simultaneous fluid mode against a variable water flow rate at a fixed air flow rate (0.055 kg/s).

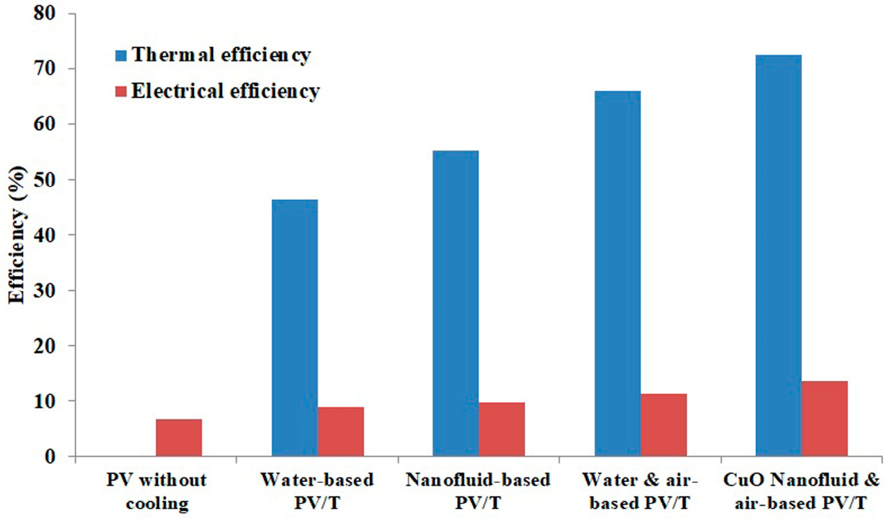

Figure 13. A performance comparison of the current system with previously reported PV/T systems.

6. Conclusions

Transient mathematical and CFD models of a nano-engineered dual-fluid PV/T system were developed in this study. To determine the optimal fluid type for the dual-fluid PV/T system, the effect of different concentrations of metal oxide nanoparticles in the base fluid was evaluated. The 0.75% CuO nanofluid showed more promising results than the other colloidal solutions evaluated herein. When the fluids are being operated simultaneously, the total energy production of a PV/T system using CuO nanofluid plus air as a dual fluid was higher than that of the water plus air case. We observed that the maximum total equivalent efficiencies of the PV/T system using the CuO nanofluid plus air, and using the water plus air, were 90.3% and 79.8%, respectively. The results showed that the heat transfer behavior of the nanofluid was highly dependent on the nanoparticle concentration. The nanofluid as a coolant tends to extract extra accumulated solar heat from the PV module even at higher operating temperature, in comparison with water. The simulation results were in good agreement with the published data. It is important to emphasize that the utilization of two fluids (nanofluid and air in particular) instead of a single fluid affects the efficiency pattern of the PV/T collector. It is anticipated that even with a very small penalty in the form of the electrical cost to pump two fluids, the decrease in the PV module temperature and the increase in the thermal efficiency of the collector are enormous. Outdoor experimental testing will be a future research focus in order to optimize the proposed collector performance.

Author Contributions: All authors contributed equally to the research work and its final decimation as an article in its current form.

Funding: This research was funded by Korea Research Fellowship Program through the National Research Foundation of Korea (NRF) funded by the Ministry of Science and ICT (2016H1D3A1938222) and The APC was funded by Korea Institute of Energy Technology Evaluation and Planning (KETEP) and the Ministry of Trade, Industry & Energy (MOTIE) of the Republic of Korea (No. 20188550000480).

Conflicts of Interest: The authors declare no conflict of interest.

Nomenclature

M	mass (kg)
C	specific heat (J/kg °C)
T	temperature (°C)
A	surface area (m^2)
h_{wind}	heat transfer coefficient due to wind (W/m^2 °C)
$h_{p\infty}$	convection heat transfer coefficient between PV & ambient air (W/m^2 °C)

h_{pt}	conduction heat transfer coefficient between PV & tube (W/m^2 °C)
h_{pa}	convection heat transfer coefficient between PV & inside air (W/m^2 °C)
h_{pb}	radiation heat transfer coefficient between PV & back panel (W/m^2 °C)
h_{tn}	convection heat transfer coefficient between tube & nanofluid (W/m^2 °C)
h_{ta}	convection heat transfer coefficient between tube & inside air (W/m^2 °C)
h_{ab}	convection heat transfer coefficient between back panel & inside air (W/m^2 °C)
E	electrical energy (W)
P	packing factor
G	solar radiation (W/m^2)
k	thermal conductivity (W/m °C)
u_a	wind velocity (m/s)
W	width or spacing (m)
x	distance (m)
D_i & D_o	tube inner & outer diameters
Nu	Nusselt number
Re	Reynolds number
Pr	Prandtl number
$\dot{m}$	mass flow rate (kg/s)
Greek	
α	absorptivity
η	efficiency
η_{PVT}	total equivalent efficiency
β_r	solar cell temperature coefficient (l/K)
ε	emissivity
σ	Stefan-Boltzman constant $\left(\mathrm{W\ m^{-2}K^{-4}}\right)$
ϕ	volume concentration of nanoparticles
Subscripts	
p	PV plate
t	absorber tube
n	nanofluid
a	inside air
b	back panel
∞	ambient air
e	electrical
r	reference
n,o & n,in	nanofluid outlet & inlet
a,o & a,in	air outlet & inlet
th	thermal
c	collector
pp	power plant
np	nanoparticles
bf	base fluid

References

1. Yazdanpanahi, J.; Sarhaddi, F.; Mahdavi Adeli, M. Experimental investigation of exergy efficiency of a solar photovoltaic thermal (PVT) water collector based on exergy losses. *Sol. Energy* **2015**, *118*, 197–208. [CrossRef]
2. Aste, N.; Del Pero, C. Simulation model for forecast of the energy performance of PV plants. In Proceedings of the ASME ATI Conference, Milano, Italy, 14–17 May 2006; Volume 2006, pp. 14–17.
3. Chow, T.T. A review on photovoltaic/thermal hybrid solar technology. *Appl. Energy* **2010**, *87*, 365–379. [CrossRef]
4. Kumar, R.; Rosen, M.A. Performance evaluation of a double pass PV/T solar air heater with and without fins. *Appl. Therm. Eng.* **2011**, *31*, 1402–1410. [CrossRef]

5. Imtiaz Hussain, M.; Ali, A.; Lee, G.H. Multi-module concentrated photovoltaic thermal system feasibility for greenhouse heating: Model validation and techno-economic analysis. *Sol. Energy* **2016**, *135*, 719–730. [CrossRef]
6. Charalambous, P.; Kalogirou, S.; Maidment, G.; Yiakoumetti, K. Optimization of the photovoltaic thermal (PV/T) collector absorber. *Sol. Energy* **2011**, *85*, 871–880. [CrossRef]
7. Mahian, O.; Kianifar, A.; Kalogirou, S.A.; Pop, I.; Wongwises, S. A review of the applications of nanofluids in solar energy. *Int. J. Heat Mass Transf.* **2013**, *57*, 582–594. [CrossRef]
8. Rejeb, O.; Sardarabadi, M.; Ménézo, C.; Passandideh-Fard, M.; Dhaou, M.H.; Jemni, A. Numerical and model validation of uncovered nanofluid sheet and tube type photovoltaic thermal solar system. *Energy Convers. Manag.* **2016**, *110*, 367–377. [CrossRef]
9. Hasan, H.A.; Sopian, K.; Jaaz, A.H.; Al-Shamani, A.N. Experimental investigation of jet array nanofluids impingement in photovoltaic/thermal collector. *Sol. Energy* **2017**, *144*, 321–334. [CrossRef]
10. Elmir, M.; Mehdaoui, R.; Mojtabi, A. Numerical simulation of cooling a solar cell by forced convection in the presence of a nanofluid. *Energy Procedia* **2012**, *18*, 594–603. [CrossRef]
11. Sardarabadi, M.; Passandideh-Fard, M.; Heris, S.Z. Experimental investigation of the effects of silica/water nanofluid on PV/T (photovoltaic thermal units). *Energy* **2014**, *66*, 264–272. [CrossRef]
12. Michael, J.J.; Iniyan, S. Performance analysis of a copper sheet laminated photovoltaic thermal collector using copper oxide–water nanofluid. *Sol. Energy* **2015**, *119*, 439–451. [CrossRef]
13. Tripanagnostopoulos, Y. Aspects and improvements of hybrid photovoltaic/thermal solar energy systems. *Sol. Energy* **2007**, *81*, 1117–1131. [CrossRef]
14. Abu Bakar, M.N.; Othman, M.; Hj Din, M.; Manaf, N.A.; Jarimi, H. Design concept and mathematical model of a bi-fluid photovoltaic/thermal (PV/T) solar collector. *Renew. Energy* **2014**, *67*, 153–164. [CrossRef]
15. Jarimi, H.; Bakar, M.N.A.; Othman, M.; Din, M.H. Bi-fluid photovoltaic/thermal (PV/T) solar collector: Experimental validation of a 2-D theoretical model. *Renew. Energy* **2016**, *85*, 1052–1067. [CrossRef]
16. Duffie, J.A.; Beckman, W.A. *Solar Engineering of Thermal Processes*, 4th ed.; John Wiley & Sons: Hoboken, NJ, USA, 2013.
17. Dubey, S.; Tiwari, G. Thermal modeling of a combined system of photovoltaic thermal (PV/T) solar water heater. *Sol. Energy* **2008**, *82*, 602–612. [CrossRef]
18. Chow, T. Performance analysis of photovoltaic-thermal collector by explicit dynamic model. *Sol. Energy* **2003**, *75*, 143–152. [CrossRef]
19. Bhattarai, S.; Oh, J.-H.; Euh, S.-H.; Krishna Kafle, G.; Hyun Kim, D. Simulation and model validation of sheet and tube type photovoltaic thermal solar system and conventional solar collecting system in transient states. *Sol. Energy Mater. Sol. Cells* **2012**, *103*, 184–193. [CrossRef]
20. Zerradi, H.; Ouaskit, S.; Dezairi, A.; Loulijat, H.; Mizani, S. New Nusselt number correlations to predict the thermal conductivity of nanofluids. *Adv. Powder Technol.* **2014**, *25*, 1124–1131. [CrossRef]
21. Maxwell, J.C. *A Treatise on Electricity and Magnetism*; Clarendon Press: Oxford, UK, 1873.
22. Drew, D.A.; Passman, S.L. *Theory of Multicomponent Fluids*; Springer Science & Business Media: Berlin, Germany, 2006; Volume 135.
23. Fluent, A. *14.0. User's and Theory Guides*; FLUENT Inc.: New York, NY, USA, 2011.
24. Khanjari, Y.; Pourfayaz, F.; Kasaeian, A. Numerical investigation on using of nanofluid in a water-cooled photovoltaic thermal system. *Energy Convers. Manag.* **2016**, *122*, 263–278. [CrossRef]
25. Imtiaz Hussain, M.; Lee, G.H. Experimental and numerical studies of a U-shaped solar energy collector to track the maximum CPV/T system output by varying the flow rate. *Renew. Energy* **2015**, *76*, 735–742. [CrossRef]
26. Ekramian, E.; Etemad, S.G.; Haghshenasfard, M. Numerical analysis of heat transfer performance of flat plate solar collectors. *J. Fluid Flow Heat Mass Transf.* **2014**, *1*, 38–42. [CrossRef]
27. Tagliafico, L.A.; Scarpa, F.; Tagliafico, G.; Valsuani, F. An approach to energy saving assessment of solar assisted heat pumps for swimming pool water heating. *Energy Build.* **2012**, *55*, 833–840. [CrossRef]
28. Hussain, M.I.; Lee, G.H. Numerical and experimental heat transfer analyses of a novel concentric tube absorber under non-uniform solar flux condition. *Renew. Energy* **2017**, *103*, 49–57. [CrossRef]
29. Vyas, A.A. CFD Based Thermal Efficiency Analysis of Solar Air Heater with Smooth Plate & Perforated Plate. *Imp. J. Interdiscip. Res.* **2017**, *3*, 415.
30. Fluent, A. *Fluent 14.0 User's Guide*; ANSYS FLUENT Inc.: Canonsburg, PA, USA, 2011.

31. Joshi, A.; Tiwari, A.; Tiwari, G.; Dincer, I.; Reddy, B. Performance evaluation of a hybrid photovoltaic thermal (PV/T)(glass-to-glass) system. *Int. J. Therm. Sci.* **2009**, *48*, 154–164. [CrossRef]
32. Faizal, M.; Saidur, R.; Mekhilef, S.; Alim, M. Energy, economic and environmental analysis of metal oxides nanofluid for flat-plate solar collector. *Energy Convers. Manag.* **2013**, *76*, 162–168. [CrossRef]
33. Al-Waeli, A.H.; Chaichan, M.T.; Kazem, H.A.; Sopian, K. Comparative study to use nano-(Al2O3, CuO, and SiC) with water to enhance photovoltaic thermal PV/T collectors. *Energy Convers. Manag.* **2017**, *148*, 963–973. [CrossRef]
34. AZO MATERIALS, A. Silica-Silicon Dioxide. Available online: https://www.azom.com/properties.aspx?ArticleID=1114 (accessed on 30 August 2018).
35. Cuce, E.; Bali, T.; Sekucoglu, S.A. Effects of passive cooling on performance of silicon photovoltaic cells. *Int. J. Low-Carbon Technol.* **2011**, *6*, 299–308. [CrossRef]